In-vitro forming of calcium phosphate layer on sol–gel hydroxyapatite-coated metal substrates

D.-M. LIU, Q. YANG, T. TROCZYNSKI
Department of Metals and Materials Engineering, University of British Columbia, Vancouver, British Columbia, Canada V6T 1Z4

In-vitro deposition of calcium phosphate layer (CPL) on metallic substrate requires special surface preparation in order to provide an interfacial bond. In this work 316 stainless steel surface is modified through deposition of a thin film ($\sim 0.5\,\mu m$) of sol–gel hydroxyapatite (SG-HA). This well-bonded film acts as an intermediary and nucleation surface of the CPL film. The SG-HA films were annealed at 375 °C (samples coded 375-ACS) and 400 °C (400-ACS) to achieve different crystallinity of the films, and thus to affect and study the CPL nucleation process. The CPL growth was investigated in terms of deposition kinetics and microstructural development. A deposition rate of dense CPL of about 0.43 μm/day was achieved on the crystallized film of 400-ACS, and 0.22 μm/day of porous CPL on amorphous 375-ACS. A compositional variation of Ca/P ratio across the CPL film thickness (400-ACS) was observed. Lower Ca/P ratio of 1.2 was detected near the substrate-CPL interface and about 1.5 near the solution-CPL interface. Infrared analysis showed the CPL to be of apatitic calcium-deficient structure. Kinetic model explaining the advancement of the CPL upon the *in-vitro* immersion is proposed.

1. Introduction

Bioactive materials such as bio-glasses, calcium hydroxyapatite (HA), tri-calcium phosphate, etc., promote bone–tissue formation at the interface and form chemical bonding with osseous tissues while they are in close contact after the materials being implanted. Such remarkable properties allow bioactive materials use in a number of medical applications in dentistry and orthopedics [1–3]. Formation of calcium phosphate layer (CPL) on the surface of the bioactive materials in solutions that mimic blood plasma has been recognized as a prerequisite for the materials to form a bond with living tissue [4, 5]. Therefore, the formation of CPL *in vitro* on the surface of the materials is considered as indicative of their bioactivity, and also allows prediction of their *in-vivo* behavior.

Biomimetic deposition process was used recently to deposit CPL films at room or body temperature for a variety of biomedical applications, including drug delivery [6, 7]. This forming mechanism is primarily driven by supersaturation of desirable ionic species, primarily Ca^{2+} and PO_4^{3-}, under an appropriate pH solution. The apatitic crystals form through nucleation and growth on specially prepared (''activated'') material surface. A direct incorporation of biological active agents, such as antibiotics, anti-cancer drugs, anti-inflammatory agents, etc., enhances clinical success of the CPL. The most attractive rationale of such biomimetic deposition process is that CPL can be developed at ambient environment, i.e. heat treatment is no longer required as opposed to other techniques such as plasma spraying [8, 9], physical/chemical vapor deposition [10–13], and sol–gel methods [14–17]. Recently, a number of reports have emphasized the formation of CPL onto metallic substrates, such as titanium (Ti) or its alloys. For instance, Wen *et al*. [18] deposited CPL onto porous Ti surface subjected to simple chemical treatments, following a pre-calcification procedure that activated the Ti surface. Deposition of CPL, at a rate as fast as 1 μm/h, has been observed. However, the deposited phase was predominantly composed of loose octacalcium phosphate plates, which had poor mechanical properties and was unsuitable for drug incorporation and release. Later, they [18] modified the process to deposit dense CPL with an apatitic structure onto the porous Ti surface at a deposition rate of about 3 μm over 8-day *in-vitro* immersion [6]. They suggested that strong adhesion of this CPL variant could be expected due to chemical bonding and mechanical entanglement of the calcium phosphate crystals on the porous surface of Ti. Campbell *et al*. [19] activated the substrate surface via a surface-induced mineralization technique, where macromolecules containing functional groups were employed to form a self-assembled monolayer on material surface. These molecules ''anchor'' to the underlying substrate and can further interact with other organic molecules with functionalized end groups that are able to induce mineral nucleation and growth. The deposition rate of CPL on such activated surface was found to be solely dependent on the solution chemistry. The deposition rates were 0.4–0.5 μm/h for solution of sufficient degree

of supersaturation (with respect to the formation of apatite crystals) and about 1 μm/day for only slightly supersaturated solution. As disclosed in a recent patent literature, drug molecules can be introduced into such CPL film via a cyclic deposition–adsorption process [7]. One promising feature of this technique is that it allows substrates of different materials to be coated with CPL. The method can be used to coat prosthetic devices with complex geometry.

Therefore, it seems conceivable that the formation of CPL imparts not only bioactive property to those biocompatible materials, e.g. native Ti surface, but may also serve for drug delivery purposes. In other words, CPL may essentially be a dual-functional coating. In this investigation, we study the formation of CPL on sol–gel hydroxyapatite (SG-HA) coated stainless steel as model substrate. Stainless steel, which is considered to be biocompatible but biologically inactive, has widely been used for screws, plates, etc., in orthopedic surgery. In a previous study, the present authors have demonstrated a process for formation of strong, adhesive HA thin layers on 316 stainless steel substrates, after low temperature annealing of 375–500 °C [20]. Crystallinity of the 0.3–0.8 μm SG-HA coatings improved with temperature of the heat treatment, yielding essentially amorphous structure at 375 °C and well crystallized phase at $\geq$ 400 °C. The coatings annealed at 375 °C and 400 °C were selected to investigate the *in-vitro* deposition of CPL. Deposition kinetics and microstructural evolution of the CPL on these substrates were explored.

2. Experimental procedures

The procedures for SG-HA coating of stainless steel substrates have been detailed elsewhere [17]. In brief, stainless steel substrates with dimensions of 1.5 cm × 1.5 cm × 0.1 cm were dip-coated into a sol–gel solution which has recently been developed for low-temperature synthesis of apatitic phase [20]. After 16 h oven drying at 80 °C, the coatings were annealed at 375 °C and 400 °C for 60 min and 20 min, respectively (these substrates are termed as ''375-ACS'' and ''400-ACS'', respectively).

The coatings of surface area of about 1.5 cm^2, were then immersed into 50 ml of a water-based fluid of composition nearly identical to that of human blood plasma, in a sealed polyethylene container. The ionic composition (in units of mmol/l) of the fluid was 142 Na^+, 5.0 K^+, 2.5 Ca^{2+}, 1.5 Mg^{2+}, 103 Cl^-, 25, HCO_3^-, 1.4 HPO_4^{2-}, and 0.5 SO_4^{2-}. This ''simulated body fluid'' (hereafter termed SBF) was buffered at pH 7.4 with tris(hydroxymethyl)aminomethane and HCl. The *in-vitro* test was performed in a static condition (i.e. the SBF was not renewed during the test period) at ambient temperature, $\sim$ 24 °C, for 14 days. The solution pH was monitored periodically and the samples of CPL were taken out at 3, 7 and 14 day periods for microstructural examination. Microstructure of the deposition layer was examined using a scanning electron microscopy (SEM, Hitachi, Model 200). For cross-sectional microstructural observation, samples were mounted in an epoxy resin (Industrial Formulators of Canada, Ltd.), thermally cured at 75 °C for 2 h, and polished down to 1 μm Al_2O_3 powder suspension. Fourier transform infrared (FTIR, Impact 400D Nicholet Spectrometer) with reflectance mode was used for phase analysis before and after the *in-vitro* test.

3. Results

3.1. Microstructural examination

Fig. 1 illustrates typical surface morphology of the crystalline CPL deposit layer grown on SG-HA film on 316 stainless steel substrate. This film shows extensive surface cracking resulting from drying of the gel-like deposit materials, as has frequently been observed in *in-vitro* studies [21, 22]. However, higher magnification micrographs, Fig. 2(a) and (b), show different morphological features on 375-ACS and 400-ACS substrates, respectively, after 14 day immersion. Loose packing of the apatite particles is observed for the 375-ACS, resulting in a pore size of about 190 nm. The equiaxial particles are uniformly distributed and are about 0.32–0.35 μm in diameter. For the 400-ACS substrate, denser packing with cauliflower-like particles is observed, Fig. 2(b). However, the apatite particles are hardly distinguishable as individual identities, as in the case of Fig. 2(a), but rather show as clusters of smaller particles of the order of about 0.1 μm. The clusters have an apparent size of about 0.4–0.5 μm, which is somewhat larger than those observed in Fig. 2(a). Few crevice-like pores, about 60 nm wide and 0.1–0.5 μm long are also present on the surface of CPL. Cross-sectional examination of the deposit layer shows an average of about 3–3.2 μm thickness for the 375-ACS substrate but 6–6.2 μm thickness for 400-ACS, as illustrated in Fig. 3(a) and (b) respectively. Whereas porous structure is seen for 375-ACS (consistent with surface morphology in Fig. 2(a)), rather dense structure is observed for the 400-ACS substrate. It should be noted that interfacial cracking appeared on 375-ACS substrate (arrow in Fig. 3(a)) possibly due to rather porous and weak particulate structure of the deposit layer. However, adhesive deposit was found for the 400-ACS substrate, Fig. 3(b). Therefore, this substrate is further characterized with more detail.

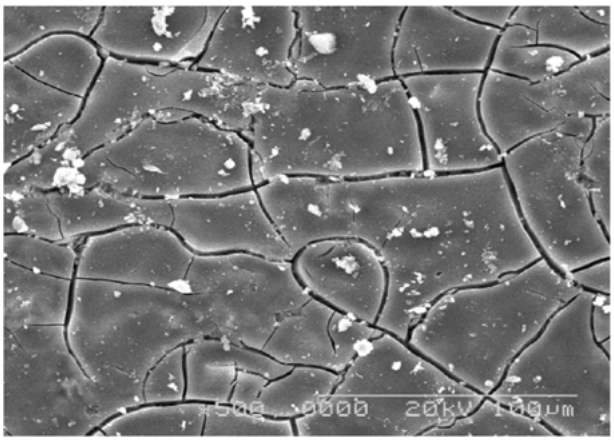

Figure 1 Surface morphology of the deposit layer.

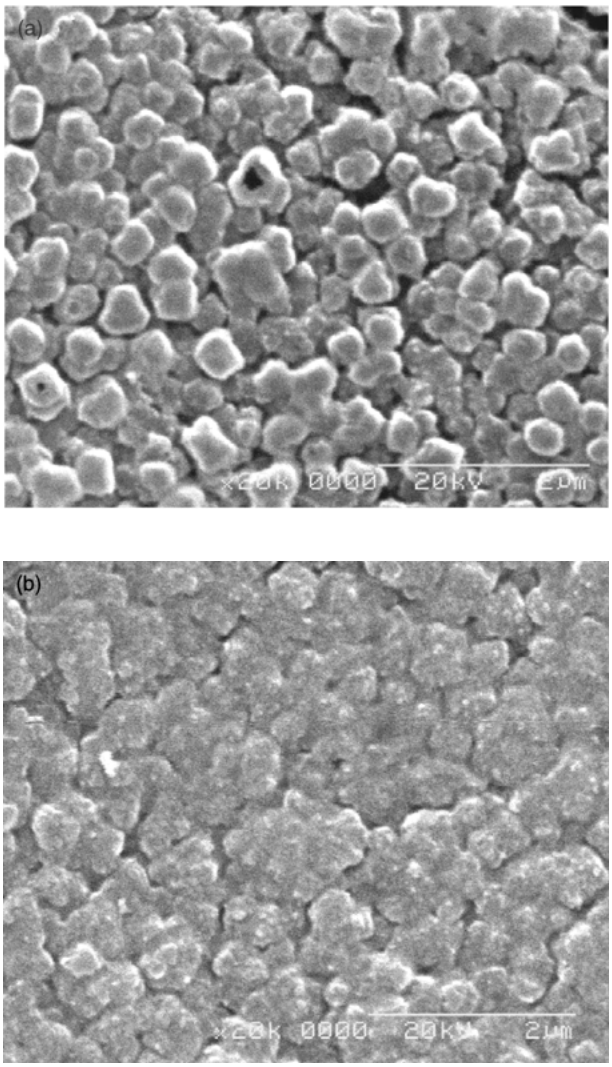

Figure 2 Surface microstructure of the deposit layer *in vitro* on (a) 375-ACS and (b) 400 ACS substrates.

3.2. IR analysis

Fig. 4(a) and (b) illustrate the FTIR spectra of the 375-ACS and 400-ACS substrates, respectively, before and after 14 days immersion. For the 375-ACS substrate, the bands at 711 cm^{-1} and 740 cm^{-1} attributed to NO_3 residue disappeared after the immersion. Instead, clearly distinct absorption bands at 563 cm^{-1} and 600 cm^{-1}, corresponding to ν_4 PO_4 groups in apatitic environment, associated with a shoulder at 630 cm^{-1}, assigned to OH groups, were detected. The presence of the above-mentioned splitting absorption bands in the region of 600–500 cm^{-1} suggests the development of crystalline apatitic structure in CPL. This is in contrast to the spectrum before immersion, where an ill-defined absorption band in the same wavenumber region was detected, indicative of amorphous or poorly crystalline apatitic structure. For the 400-ACS substrate, Fig. 4(b), the ''after immersion'' IR spectrum is identical to that of 375-ACS. The residual NO_3 groups also disappeared as a result of dissolution. However, the absorption bands at 600–500 and 1100–950 cm^{-1} regions corresponding to the PO_4 groups remain unchanged after the immersion, suggesting that the deposit crystals have similar crystalline structure as the underlying SG-HA. A broad band over the region of 1500–1400 cm^{-1} together with an absorption band at 871 cm^{-1} appearing after immersion suggests incorporation of carbonate groups in the apatite crystals, indicating that the deposit layer is essentially carbonated apatite, resembling that of human mineralized tissue.

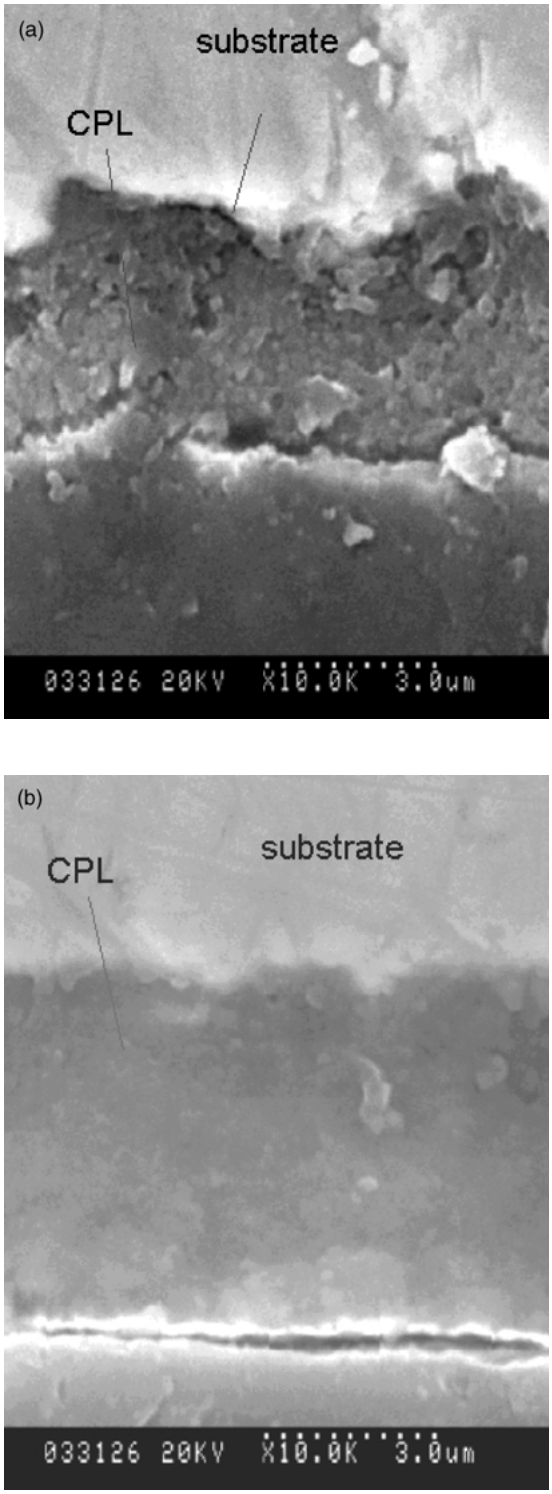

Figure 3 Cross-sectional view of the deposit layer on (a) 375-ACS and (b) 400-ACS substrates.

3.3. Deposit formation

Fig. 5(a), (b), and (c) show the microstructural evolution of the top surface of the CPL deposit layer on the 400-ACS substrate after 3, 7, and 14 days immersion, respectively. It is apparent that the deposit layer covered

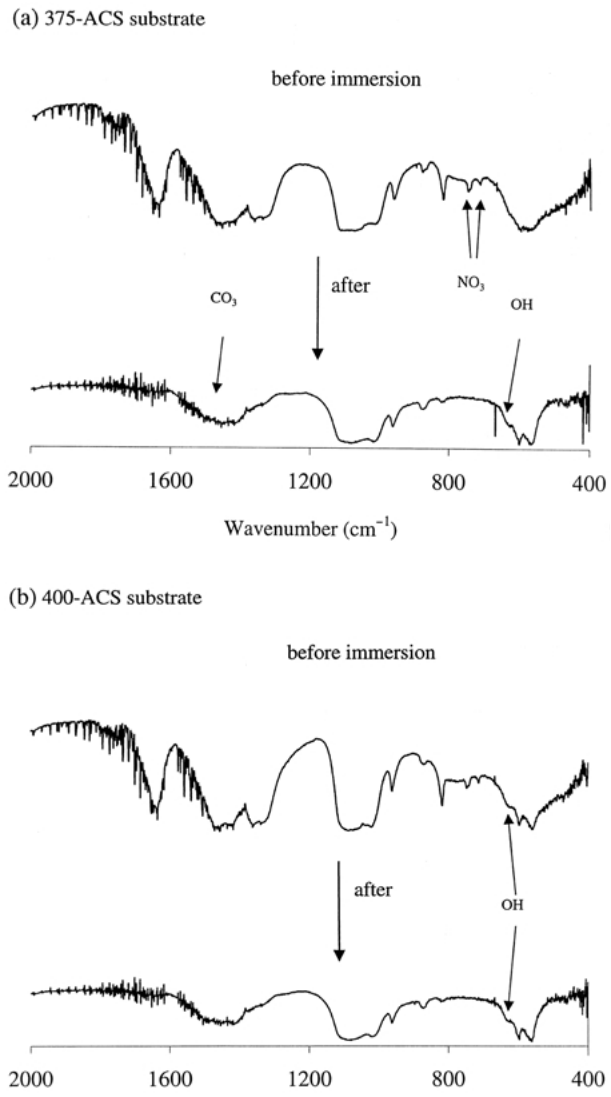

Figure 4 FTIR spectra for the (a) 375-ACS and (b) 400-ACS substrates before and after the *in-vitro* immersion test, at a time period of 14 days.

most of the surface area of the substrate already after 3 days of immersion. Few surface pores are present in the deposition layers. A close examination of the pore structure indicates that these pores develop as a result of poor assembly of smaller particles, i.e. the deposit layer is essentially an assembly of small spherical particles of about 100–150 nm in diameter. These small particles remained nearly identical in size and shape over the entire time frame of immersion, suggesting a constant crystal growth rate and unchanged growth mechanism over the immersion duration.

The deposit layer thickness (H_{CPL}) increases with time (t) according to nearly linear relationship, Fig. 6, and Equation 1:

$$H_{\mathrm{CPL}} = k't \tag{1}$$

The correlation coefficient $R^2 = 0.995$ and 0.988 for 375-ACS and 400-ACS substrates, respectively. The slope (k', referred to as a rate constant) suggests a constant deposition rate, $k'_{375} = 0.22\,\mu$m/day for the 375-ACS and $k'_{400} = 0.43\,\mu$m/day for the 400-ACS. The latter shows a deposition rate slightly faster than that observed by Wen *et al*. [6] who imparted the bioactive property on surface of Ti and Ti alloy through a two-step

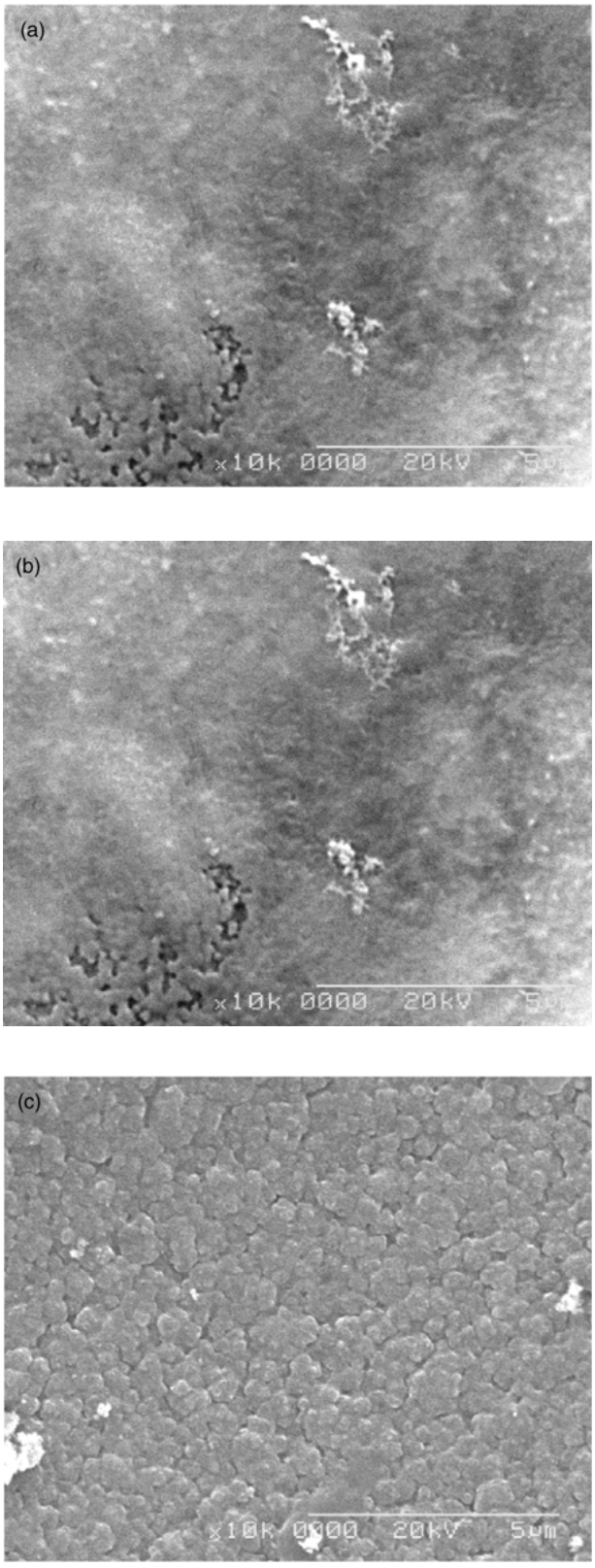

Figure 5 Close examination on the surface microstructural evolution on the 400-ACS substrate for an immersion time period of (a) 3, (b) 7, and (c) 14 days.

chemical modification. It should be noted that the solid lines in Fig. 6 intercept the point near the origin, suggesting a relative short induction time for calcium phosphate nuclei to develop on the SG-HA layer, consistent with findings of Radin and Ducheyne [23]. The linear deposition rate allows control of the thickness of CPL, which may benefit certain specific designs, such as a drug-apatite-drug multi-layer structure.

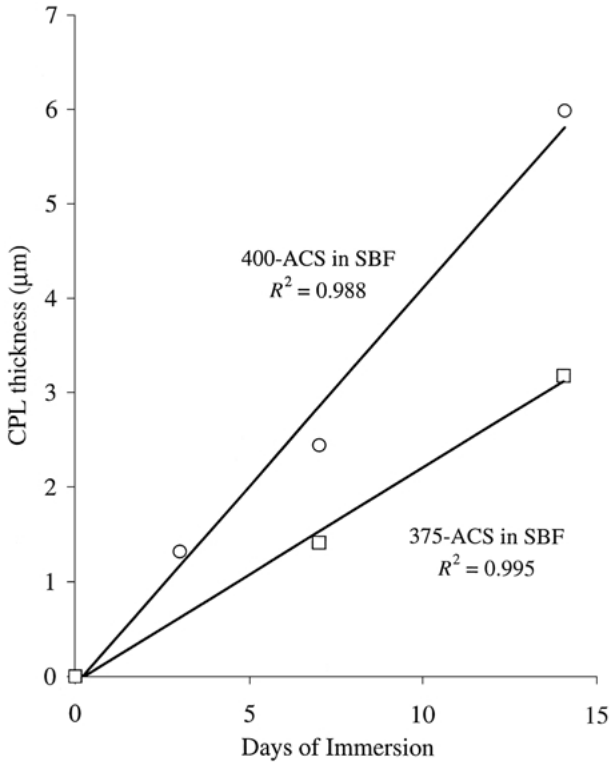

Figure 6 Deposit layer thickness in terms of time of immersion, showing a linear relationship for both substrates.

Energy dispersive spectroscopy (EDS) along the CPL on the 400-ACS substrate shows an increase in Ca/P ratio from 1.20 at the region 1 μm above the interface to 1.55 at 1 μm below the outermost layer was detected for the 400-ACS substrate, Fig. 7. These findings suggest that the apatitic CPL is calcium-deficient, which is similar to that of the underlying SG-HA thin film [20].

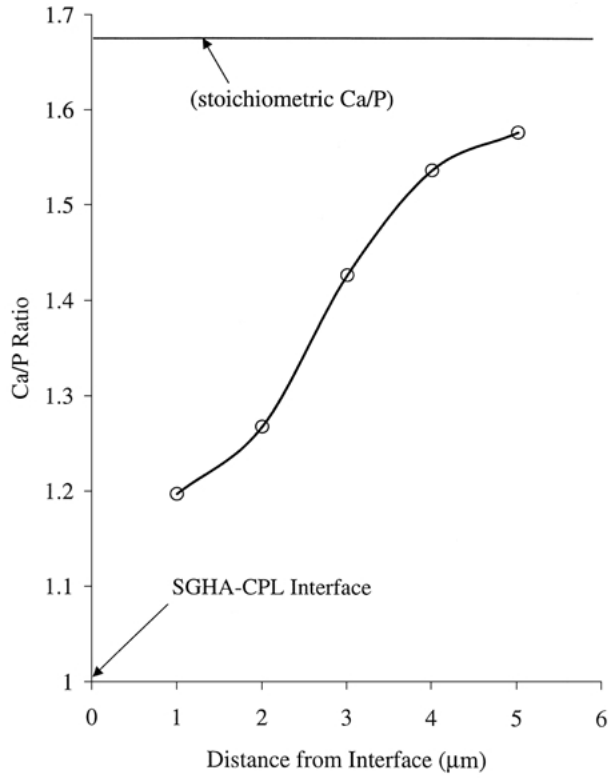

Figure 7 The variation of the Ca/P ratio along the deposit layer, where an increased Ca/P ratio was found as the layer keeps growing.

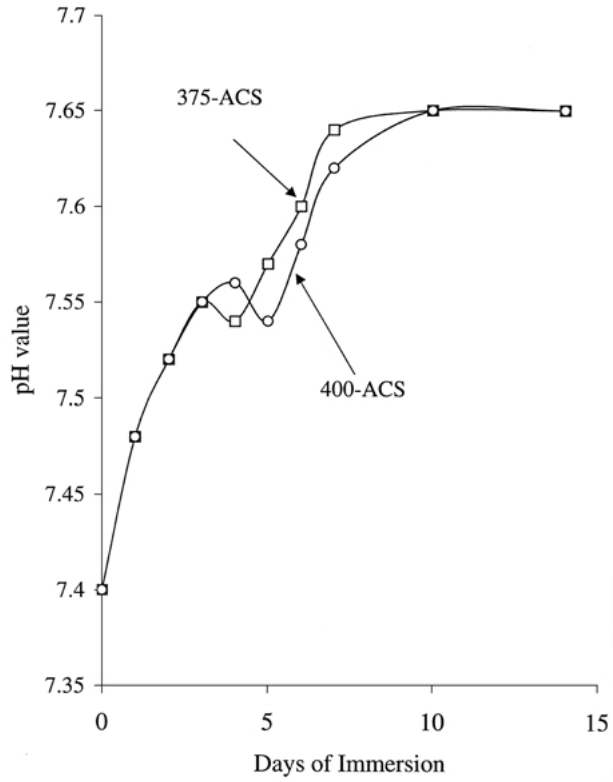

Figure 8 The pH level of the SBF is increased with the time of immersion and reaches plateau after about 10 days of test.

Measurement of the pH level of the SBF during deposition indicates that the solution pH increases with immersion time, as shown in Fig. 8. This increase in solution pH with immersion time may explain the resulting increased Ca/P ratio of the deposit, where more Ca^{2+} ions adsorbed on the more negatively charged surface (i.e. in the higher pH environment) [21, 24, 25]. This followed with incorporation of phosphate ions to form precipitate on the surface, resulting in the CPL with an increased Ca/P ratio with immersion time.

4. Discussion

Calcium phosphate minerals are unable to nucleate and grow on native metallic surfaces, e.g. Ti alloys or stainless steel, typically used for biomedical devices. At the same time *in-vitro* deposition of the films at near-ambient temperature opens up a possibility for drug encapsulation to affect tissue response to the surface, e.g. of an implant. Therefore, modification of such native metallic surfaces is necessary, and has been undertaken in the past using variety of chemical and/or physical treatments. In this work the formation of apatite-like layer (CPL) on stainless steel has been imparted onto the surface through a pre-coated thin layer of apatite using sol–gel route. This result suggests that such an *in-vitro* surface bioactivity can be proposed as the prerequisite for *in-vivo* bond formation [4].

The formation of calcium phosphate deposit has been well recognized as a result of nucleation-growth mechanism on substrate surface. However, it is critical to form a CPL, rather than discrete particles, on the substrate. In a recent study, Wen *et al*. [6] observed various modes of CPL deposit, from discrete particles to

uniform Ca–P layer, on chemically modified Ti or Ti alloys surfaces after 14 days immersion into Hank's balance salt solution. The solution had Ca^{2+} and HPO_4^{2-} concentration about half of that used in the present protocol. The CPL formation was controlled by the nucleation sites present on the metal surface, a function of surface topology [26] and surface OH^- groups [24]. The latter can be understood as a result of Ca^{2+} adsorption, following interaction with the surrounding phosphate ions to form calcium phosphate precipitates.

In this work we have undertaken an entirely different approach to surface modification of metallic substrates to encourage *in vitro* deposition of calcium phosphates, i.e. through deposition of an intermediate thin HA film using sol–gel technology. The interfacial SG-HA (0.3–0.6 μm thin apatite) coating showed high biological activity by inducing formation of a uniform layer of CPL, starting immediately after immersion. However, for the 375-ACS substrate, a porous CPL deposited with a rate slower than the 400-ACS substrate, suggesting a poorer bioactivity of the 375-ACS. Close examination of the IR spectra of the 400-ACS substrates before the immersion reveals a discernable shoulder at $630\,cm^{-1}$, corresponding to vibrational mode of OH^- groups in the apatite structure. This shoulder band became weaker (but can still be seen) for the 375-ACS substrate. As OH^- groups attract Ca^{2+} ion in the solution, improved biological activity is expected for the 400-ACS substrate. Therefore, higher population of the OH^- groups on the substrates indicates greater amount of nucleation sites for CPL. This could be the reason why a denser CPL structure developed on the 400-ACS substrate as compared to the 375-ACS substrate (Fig. 2). The growth of nuclei in a direction parallel to the substrate surface would be constrained because of the abundant nucleation sites.

This hypothesis may explain both the faster deposition rate and an assembly of particulate clusters observed on the 400-ACS substrate. The observed deposition rate of CPL may be related to the growth kinetics of the nuclei once they were stably developed on the surface. According to classic kinetics of surface controled crystal growth process, the overall crystal growth rate is a combination of bulk diffusion and surface reaction. Mullin [27] expressed such a surface mineralization by simple empirical equation;

$$R = ks\sigma^n \tag{2}$$

where the growth rate (R) is a function of k, kinetic constant, s is a parameter proportional to the number of growth sites (m) on the surface, and σ is the relative supersaturation ratio. The exponent n is the order of reaction, i.e. for surface reaction controlled growth, $n = 2$, and for a bulk diffusion controlled process, $n = 1$. In a recent study, Combes *et al*. [28] investigated the growth kinetics of CPL on Ti particles and defined crystal growth rate (R) as:

$$R = \frac{(\Delta VC)}{(\Delta t m_0 A_s)} \tag{3}$$

where $\Delta V/\Delta t$ represents the weight change of the particulate substrate of initial weight m_0 and surface area A_s during deposition, and C is the effective concentration of the solution with respect to the deposit phase. By analogy to the growth rate of the deposit phase, Equation 3 can be modified and used for current study by taking the term $\Delta V/\Delta t$ as a $\Delta H_{CPL} A_{CPL} \rho_{CPL}/\Delta t$, where A_{CPL} is the surface area of the deposit phase on the model substrate and is the same as A_s for dense structure, and ρ_{CPL} is the density of the deposit layer. Therefore, Equation 3 can be rearranged as:

$$R = \frac{\Delta H_{CPL}}{\Delta t} \quad \frac{A_{CPL}\rho_{CPL}C}{m_0 A_s} \tag{4}$$

In combination with Equation 1, Equation 4 becomes

$$R = k' \ \frac{A_{CPL}\rho_{CPL}C}{m_0 A_s} \tag{5a}$$

or for dense deposit structure,

$$R = k' \ \frac{\rho_{CPL}C}{m_0} \tag{5b}$$

It is apparent from Equation 5a or 5b that the crystal growth rate (R) in current system is constant over the immersion time period of study, as all the parameters, in particular k', appear to be constant. The observed uniform size and shape of the deposited particles is supporting evidence. Furthermore, since the $k'_{400} \cong 2k'_{375}$, it is reasonable to expect that $R_{400} \cong 2R_{375}$, indicating that the crystal growth rate on the 400-ACS substrate is nearly double that on the 375-ACS substrate. This means that a coarser grain size should be attained for the 400-ACS than that for the 375-ACS, in a given time period of deposition, and this is consistent with surface microstructural evolution observed in Fig. 2. However, as aforementioned, higher population of the nucleation sites on the 400-ACS substrate would limit the crystal size in direction parallel to the substrate surface, leading to a higher growth rate perpendicular to the substrate surface. Further nucleation and growth on the surface of the deposit crystals results in a cluster-like surface morphology (Figs 5(c) or 2(b)).

According to Equation 2, crystal growth rate (R) should be proportional to the number of nucleation sites (m) on the substrate surface because both k' and σ are constant under current experimental conditions. Therefore, by analogy, $m_{400} \cong 2m_{375}$, i.e. nearly twice as many nucleation sites developed on the 400 °C-annealed substrate than on that prepared at 375 °C. This is in good agreement with previous observation on the OH groups, possibly acting as nucleation sites, via analysis of the IR spectra, Fig. 4. This is only a qualitative observation, as it is difficult to determine if there are about twice as much as OH groups on the 400-ACS substrate in comparison to the 375-ACS substrate.

It should be particularly noted that the analysis given above should only be valid during the earlier (or initial) stage of immersion, where the nature of substrate surface is significant on deposition. Once the first layer was developed, further nucleation and growth of the calcium phosphate crystals should rely solely on the physical and chemical properties of the ''first'' layer, rather than the original substrate surface. In other words, attention should be focused on the growth of calcium phosphate

crystals on the CPL. However, microstructural examination as revealed in Fig. 3 suggests the growth of the CPL is exceptionally microstructurally consistent across the layer for each case. This implies that a subsequent nucleation and particularly growth of the calcium phosphate crystals on the ''first'' layer of CPL would be identical to that occurred in developing the ''first'' layer. If this assumption is true, then we believe further deposition of the ''second'' or subsequent layer should merely be a repeating mechanism as occurred in the first one if the surrounding environmental conditions held constant. In other words, within the scope of the present deposition control, the first layer may bear either microstructurally or energetically the message from starting substrate surface, allowing further growth of the CPL to be operated in the same manner.

The compositional variation of Ca/P ratio from 1.20 to 1.55 across thickness of the CPL may be caused, as previously suggested, by increasing solution pH during the deposition. However, dissolution of residual nitrate from the SG-HA films (as indicated by IR spectra in Fig. 4), may locally decrease pH, especially near the region slightly above the substrate-SBF interface. Such a localized pH reduction may lower Ca/P ratio in the CPL, since it would favor the formation of acidic calcium phosphate deposits (i.e. with lower Ca/P), especially in early period of deposition. The Ca/P ratio increases rapidly for CPL thickness between 2 μm and 4 μm (i.e. during a growth time period of 4–10 days), Fig. 7. Subsequently, Ca/P increase is slower, which may reflect equilibration of the film with the corresponding solution (as confirmed by pH monitoring, Fig. 8). This observation may be utilized to tune the Ca/P ratio to a desirable value during CPL formation via adjusting solution pH, i.e. higher solution pH promotes CPL with higher Ca/P ratio, and vice versa.

5. Concluding remarks

This investigation illustrates novel approach to improve integrity of bioactive calcium phosphate films deposited on metallic surfaces at room temperature. We have developed *in vitro* deposition of CPL onto stainless steel substrates pre-coated with sol–gel submicron apatite film. Such a thin apatite film allows the substrates to gain significant bioactivity *in vitro* by forming calcium phosphate deposit on the substrate. This also provides the capability of forming bond with living tissue *in vivo*. Microstructural analyzes indicate that the substrates coated with sol–gel apatite film and heat treated at 400 °C form adhesive, dense nano-structured CPL at a deposition rate of 0.43 μm/day. The sol–gel apatite films prepared at 375 °C formed more porous CPL at a rate of 0.22 μm/day. It is proposed that the sol–gel apatite films heat treated at 400 °C provided higher density of nucleation sites, associated with higher population of OH groups on the apatite surface. A further analysis based on a modified kinetic model provides support. The resulting CPL is essentially a CO_3- and possibly HPO_4-containing calcium-deficient apatite, chemically and structurally resembling that of mineralized tissues found in human bone and enamel.

This study suggests that *in vitro* bioactivity of metallic surface can be achieved by pre-coating it with a thin apatite film through the sol–gel process. The sol–gel film properties do affect microstructural development and stoichiometry of the CPL. Such *in vitro* deposited CPL can be used as a vehicle for therapeutically active agents for a variety of biomedical applications.

Acknowledgments

The authors are indebted to the Natural Sciences and Engineering Council Canada for supporting this work.

References

1. L. L. HENCH, *J. Am. Ceram. Soc.* **74** (1991) 1487–1510.
2. M. JARCHO, *Clin. Orthop.* **157** (1981) 259–78.
3. R. Z. LEGEROS, *Adv. Dent. Res.* **2** (1988) 164–168.
4. C. OHTSUKI, T. KOKUBO and T. YAMAMURU, *J. Non-Cryst. Solids* **143** (1992) 84–92.
5. P. DUCHEYNE, S. RADIN and K. ISHIKAWA, in ''Bone-Bonding Biomaterials'', edited by P. Duchenye, T. Kokubo and C. A. van Blitterswijk (Reed Healthcare Communications, Leiderdrop, 1992) pp. 213–18.
6. H. B. WEN, J. R. DE WIJN, F. Z. CUI and K. DE GROOT, *J. Biomed. Mater. Res.* **41** (1998) 227–36.
7. S. LIN and A. A. CAMPBELL, US patent #5 958 430 (1999).
8. D. M. LIU, H. M. CHOU and J. D. WU, *J. Mater. Sci. Mater. Med.* **5** (1994) 147–153.
9. K. DE GROOT, R. G. T. GREESINK, C. P. A. T. KLEIN and P. SEREKIAN, *J. Biomed. Mater. Res.* **21** (1987) 1375–1381.
10. P. DUCHEYNE, W. VAN RAEMDONCK, J. C. HEUGHEBAERT and M. HEUGHEBAERT, *Biomaterials* **11** (1990) 244.
11. S. BAN and S. MARUNO, *Jpn. J. App. Phys.*, part 2, Letters, **32**[10B] (1993) 1577–80.
12. C. M. COTELL, *App. Surf. Sci.* **69** (1993) 140–48.
13. L. TORRISI and G. FOTI, *App. Phys. Letters* **62** (1993) 237–39.
14. C. S. CHAI, B. BEN-NISSAN, S. PYKE and L. EVANS, *Mater. Manuf. Processes* **10** (1995) 205–216.
15. C. M. LOPATIN, V. PIZZICONI, T. L. ALFORD and T. LAURSEN, *Thin Solid Films* **326** (1998) 227–232.
16. W. WENG and J. L. BAPTISTA, *J. Mater. Sci. Mater. Med.* **9** (1998) 159–163.
17. D. M. LIU, T. TROCZYNSKI and W. J. TSENG, *Biomaterials* (in press, 2001).
18. H. B. WEN, J. G. C. WOLKE, J. R. DE WIJN, Q. LIN, F. Z. CUI and K. DE GROOT, *ibid.* **18** (1997) 1471–78.
19. A. A. CAMPBELL, G. E. FRYXELL, J. C. LINEHAN and G. L. GRAFF, *J. Biomed. Mater. Res.* **32** (1996) 111–118.
20. D. M. LIU, Q. YANG and T. TROCZYNSKI, *Biomaterials* (in press, 2001).
21. P. LI, C. OHTSUKI, T. KOKUBO, K. NAKANISHI, N. SOGA and K. DE GROOT, *J. Biomed. Mater. Res.* **28** (1994) 7–15.
22. Y. ABE, T. KOKUBO and T. YAMAMURU, *Materials in Medicine* **1** (1990) 233–238.
23. S. R. RADIN and P. DUCHEYNE, *J. Biomed. Mater. Res.* **27** (1993) 35–45.
24. H. P. BOEHM, *Disc. Faraday Soc.* **52** (1971) 264–275.
25. K. E. HEALY and P. DUCHEYNE, *Biomaterials* **13** (1992) 553–61.
26. S. MANN, B. R. HEYWOOD, S. RAJAM and V. J. WALE, in ''Mechanism and Phylogeny of Mineralization in Biological Systems'', edited by S. Suga and H. Nakahara (Springer-Verlag, Tokyo, 1991) pp. 47–55.
27. J. W. MULLIN, ''Crystallization'', 2nd edn. (Butterworths, London, 1972) p. 189.
28. C. COMBES, M. FRECHE, C. REY and B. BISCANS, *Materials in Medicine* **10** (1999) 231–237.

Received 4 June
and accepted 23 October 2001